Electronic Supporting Information

Hydroxido Supported and Differently Networked Octanuclear Ni_6Ln_2 [Ln = Gd^{III} and Dy^{III}] Complexes: Structural Variation, Magnetic Properties and Theoretical Insights

Avik Bhanja,[a] Lucy Smythe,[b] Radovan Herchel,[c] Ivan Nemec,[c] Mark Murrie,[b] Debashis Ray*,[a]

[a] *Department of Chemistry, Indian Institute of Technology, Kharagpur 721302, India*

[b] *School of Chemistry, University of Glasgow, University Avenue, Glasgow G12 8QQ, U.K.*

[c] *Department of Inorganic Chemistry, Faculty of Science, Palacky University, 17. listopadu 12, CZ-771 46 Olomouc, Czech Republic*

*E-mail: dray@chem.iitkgp.ac.in

Contents

Table S1 Crystallographic data and refinement details for complexes **1**−**2**

parameters	**1**	**2**
Formula	$C_{65}H_{95}Gd_2N_4Ni_6O_{38}$	$C_{64}H_{84}Cl_6Dy_2N_4Ni_6O_{26}$
F.W.(g mol^{-1})	2207.11	2215.24
crystal system	triclinic	monoclinic
space group	$P\bar{1}$	C 2/c
Crystal color	Green	Green
Crystal size/mm^3	0.23×0.16×0.11	0.16×0.14×0.12
a/ Å	11.53(2)	27.705(6)
b/ Å	14.72(2)	13.771(3)
c/ Å	15.378(19)	23.455(5)
α/ deg	113.93(2)	90.00
β/ deg	103.87(6)	115.55(3)
γ/ deg	102.08(5)	90.00
V/ Å^3	2174(6)	8074(4)
Z	1	4
limiting indices	$-14 \le h \le 14$ $-18 \le k \le 18$ $-19 \le l \le 16$	$-32 \le h \le 28$ $-16 \le k \le 16$ $-27 \le l \le 27$
D_c/g cm^{-3}	1.674	1.770
μ (mm^{-1})	2.846	3.344
F(000)	1033	4139
T/K	114	112
Total reflections	34276	47149
R(int)	0.0585	0.0682
Unique reflections	8932	7168
Observed reflections	5607	5685
Parameters	529	490
R_1; wR_2 ($I > 2\sigma(I)$)	0.0516, 0.1445	0.0482, 0.1257
GOF (F^2)	1.038	1.045
Largest diff peak and hole (e Å^{-3})	1.211, −1.677	1.349, −0.891
CCDC No.	2021668	2021678

Refinement of Experimental Crystallographic Data

In complex **1**, the acetato ligand was modelled as disordered over two positions (ratio of occupation factors = 0.5:0.5). One of the coordination sites of the Ni1 atom shows substitutional disorder between the aqua and methanol ligands (ratio of occupation factors = 0.5:0.5). In **2**, the co-crystallized methanol molecules exhibited positional disorder over two positions with ratio of occupation factors 0.71:0.29. The sixth coordination site of the Ni1 atom is coordinated by both methanol and water molecules and this was refined as positional disorder (CH_3OH:H_2O = 0.6:0.4). The refinement of the peripheral {$NiCl_3$} moiety (Ni3-Cl1-

Cl2-Cl3) with full occupancy led to negative densities in differential maps. Decrease of the occupation factor of the Cl2-Ni3-Cl3 fragment to 0.8 (based on previous free refinement) led to substantial improvement of the structural model. However, for the bulk sample, neither any other analytical methods nor magnetic characterization (vide infra) supports partial occupation of this fragment. It must be also noted that lowering occupancy of Cl1 to ca. 0.9 is slightly improving the structural model, but this would lead to formal charge imbalance and therefore, we preferred chemical soundness of the structural model. Furthermore, the density maxima in the vicinity of the $\{NiCl_3\}$ moiety indicates its possible positional disorder, but this was not possible to model reasonably and only disorder of the bridging Cl1 atom was established (ratio of occupation factors 0.8:0.2). A rational explanation thus may be related to the existence of several sub-sites of the Cl2-Ni3-Cl3 fragment, which adopt different orientations than the major site with occupancy 0.8.

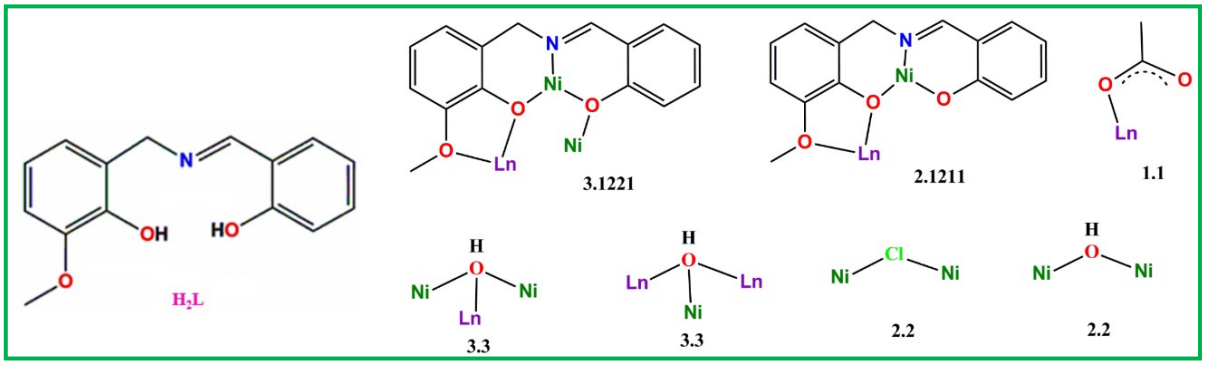

Fig. S1 Adjacent metal ion binding sites of H_2L; experimentally identified metal ion binding modes[S1] of L^{2-}, HO^-, AcO^- and Cl^-

Table S2 Results of Continuous Shape Measures (CShM)[S2-S3] using SHAPE 2.1 for Ni^{II} centres of **1**.[a]

	JPPY-6	TPR-6	OC-6	PPY-6	HP-6
Ni1 of **1**	29.524	13.577	**0.544**	26.433	29.751
Ni2 of **1**	30.937	14.516	**0.325**	27.604	30.237
Ni3 of **1**	29.062	14.245	**0.646**	25.801	27.122
Ni1 of **2**	26.499	12.031	**0.937**	22.787	28.712
Ni2 of **2**	29.941	15.346	**1.386**	26.955	31.868

[a]*JPPY-6 = Johnson pentagonal pyramid J2, TPR-6 = Trigonal prism, OC-6 = Octahedron, PPY-6 = Pentagonal pyramid, HP-6 = Hexagon*

Table S3 Results of Continuous Shape Measures (CShM)[S2-S3] using SHAPE 2.1 for Gd^{III} centres of **1**[a]

[ML9]	EP-9	OPY-9	HBPY-9	JTC-9	JCCU-9	CCU-9	JCSAPR-9	CSAPR-9	JTCTPR-9	TCTPR-9	JTDIC-9	HH-9	**MFF-9**
Gd1 of **1**	35.585	23.584	17.079	15.995	9.136	7.997	3.047	2.410	4.415	3.004	13.251	8.346	**2.087**

[a]*EP-9 = Enneagon, OPY-9 = Octagonal pyramid, HBPY-9 = Heptagonal bipyramid, JTC-9 = Johnson triangular cupola J3, JCCU-9 = Capped cube J8, CCU-9 = Spherical-relaxed capped cube, JCSAPR-9 = Capped square antiprism J10, CSAPR-9 = Spherical capped square antiprism, JTCTPR-9 = Tricapped trigonal prism J51, TCTPR-9 = Spherical tricapped trigonal prism, JTDIC-9 = Tridiminished icosahedron J63, HH-9 = Hula-hoop, MFF-9 = Muffin*

Table S4 Results of Continuous Shape Measures (CShM)[S2-S3] using SHAPE 2.1 for Dy^{III} centres of **2**.[a]

[ML8]	OP-8	HPY-8	HBPY-8	CU-8	SAPR-8	**TDD-8**	JGBF-8	JETBPY-8	JBTPR-8	BTPR-8	JSD-8	TT-8
Dy1 of **2**	33.456	22.042	12.385	5.892	2.541	**0.835**	15.884	27.900	3.442	3.210	3.489	6.323

[a]*OP-8 = Octagon, HPY-8 = Heptagonal pyramid, HBPY-8 = Hexagonal bipyramid, CU-8 = Cube, SAPR-8 = square antiprism, TDD-8 = Triangular dodecahedron, JGBF-8 = Johnson gyrobifastigium J26, JETBPY-8 = Johnson elongated triangular bipyramid J14, JBTPR-8 = Biaugmented trigonal prism J50, BTPR-8 = Biaugmented trigonal prism, JSD-8 = Snub diphenoid J84, TT-8 = Triakis tetrahedron*

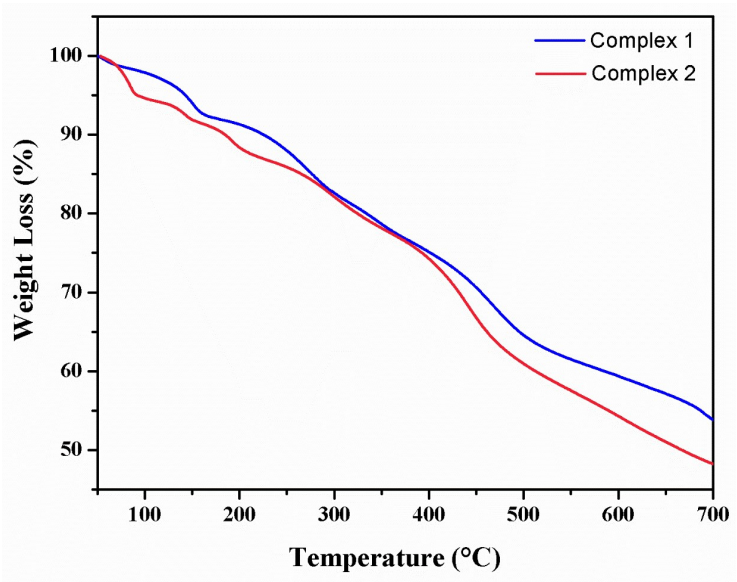

Fig. S2 TGA curves of complexes **1** and **2**. The % of weight loss in the temperature range 70°–140°C for complex **1**: 6.20% and for complex **2**: 6.85%.

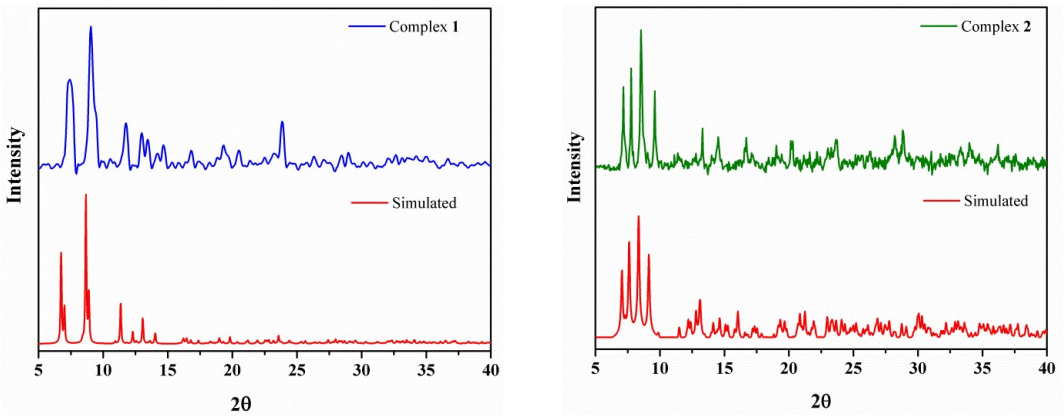

Fig. S3 Comparison of PXRD patterns of complexes **1** and **2**

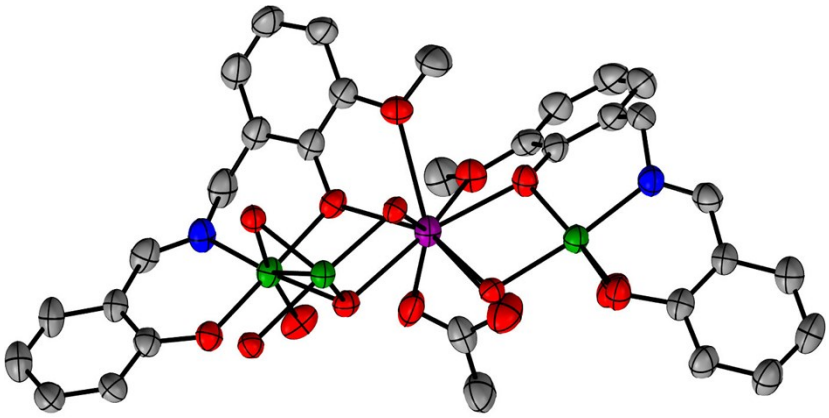

Fig. S4 The ORTEP plot of asymmetric unit in **1** with displacement ellipsoids drawn at 50% probability level. The hydrogen atoms were omitted for clarity.

Table S5 Selected bond distances (Å) of **1**

Atom 1	Atom 2	Distance		Atom 1	Atom 2	Distance
Gd1	O11	2.383(5)		Ni1	O7	2.201(6)
Gd1	O12	2.390(9)		Ni2	O11	2.077(6)
Gd1	O9	2.389(6)		Ni2	O10	2.146(6)
Gd1	O8	2.382(7)		Ni2	O5	2.042(6)
Gd1	O2	2.323(6)		Ni2	O6	1.982(6)
Gd1	O5	2.319(7)		Ni2	O15	2.089(6)
Gd1	O1	2.626(6)		Ni2	N2	1.997(8)
Gd1	O4	2.545(6)		Ni3	O11	2.030(6)
Ni1	O14	2.111(7)		Ni3	O10	2.134(6)
Ni1	O8	2.058(5)		Ni3	O9*	2.064(5)

Ni1	O2	2.039(7)		Ni3	O9	2.051(6)
Ni1	O3	1.997(6)		Ni3	O8	2.018(6)
Ni1	N1	1.989(7)		Ni3	O7	2.169(6)

Table S6 Selected bond angles (°) of **1**

Atom 1	Atom 2	Atom 3	Angles		Atom 1	Atom 2	Atom 3	Angles
O11	Gd1	O12	97.3(3)		N1	Ni1	O3	91.8(3)
O11	Gd1	O9	70.21(18)		N1	Ni1	O7	100.4(3)
O11	Gd1	O1	129.31(19)		O11	Ni2	O10*	81.4(2)
O11	Gd1	O4	123.78(19)		O11	Ni2	O1	5 92.6(2)
O12	Gd1	O9	143.4(2)		O5	Ni2	O11	82.3(2)
O12	Gd1	O1	132.0(3)		O5	Ni2	O10*	88.1(2)
O12	Gd1	O4	74.5(3)		O5	Ni2	O15	92.2(3)
O9	Gd1	O1	74.22(17)		O6	Ni2	O11	94.6(2)
O9	Gd1	O4	141.4(2)		O6	Ni2	O10*	86.4(2)
O8	Gd1	O11	84.60(17)		O6	Ni2	O5	174.1(2)
O8	Gd1	O12	74.5(3)		O6	Ni2	O15	93.0(3)
O8	Gd1	O9	70.20(19)		O6	Ni2	N2	90.6(3)
O8	Gd1	O1	115.6(2)		O15	Ni2	O10*	173.9(2)
O8	Gd1	O4	140.14(18)		N2	Ni2	O11	173.9(3)
O2	Gd1	O11	154.03(19)		N2	Ni2	O10*	95.6(3)
O2	Gd1	O12	79.3(3)		N2	Ni2	O5	92.3(3)
O2	Gd1	O9	97.13(18)		N2	Ni2	O15	90.4(3)
O2	Gd1	O8	69.6(2)		O9	Ni3	O10	176.09(19)
O2	Gd1	O1	63.8(2)		O9*	Ni3	O10	91.8(2)
O2	Gd1	O4	80.5(2)		O9*	Ni3	O9	87.1(2)
O5	Gd1	O11	70.36(19)		O9*	Ni3	O7	177.63(19)
O5	Gd1	O12	115.4(3)		O9	Ni3	O7	94.8(2)
O5	Gd1	O9	93.30(18)		O8	Ni3	O11*	173.52(19)
O5	Gd1	O8	153.75(18)		O8	Ni3	O10	91.8(2)
O5	Gd1	O2	134.5(2)		O8	Ni3	O9	84.8(2)
O5	Gd1	O1	77.0(2)		O8	Ni3	O9*	99.6(2)

O5	Gd1	O4	64.6(2)		O8	Ni3	O7	82.0(2)
O4	Gd1	O1	70.22(19)		Ni3	O9	Gd1	101.8(2)
O14	Ni1	O7	169.9(2)		Ni3	O9*	Gd1*	102.2(2)
O8	Ni1	O14	89.7(3)		Ni3	O9	Ni3*	92.9(2)
O8	Ni1	O7	80.3(2)		Ni3	O8	Gd1	103.1(2)
O2	Ni1	O14	91.0(3)		Ni3	O8	Ni1	101.8(2)
O2	Ni1	O8	81.9(2)		Ni1	O8	Gd1	102.8(2)
O2	Ni1	O7	88.7(2)		Ni1	O2	Gd1	105.5(2)
O3	Ni1	O14	94.2(3)		Ni2	O5	Gd1	105.3(2)
O3	Ni1	O8	94.6(2)		Ni3	O7	Ni1	92.8(2)
O3	Ni1	O2	173.8(2)		Ni3	O11*	Gd1*	103.4(2)
O3	Ni1	O7	85.7(2)		Ni3	O11*	Ni2*	98.9(2)
N1	Ni1	O14	89.7(3)		Ni2	O11	Gd1	102.0(2)
N1	Ni1	O8	173.6(3)		Ni3	O10	Ni2*	93.7(2)
N1	Ni1	O2	91.7(3)					

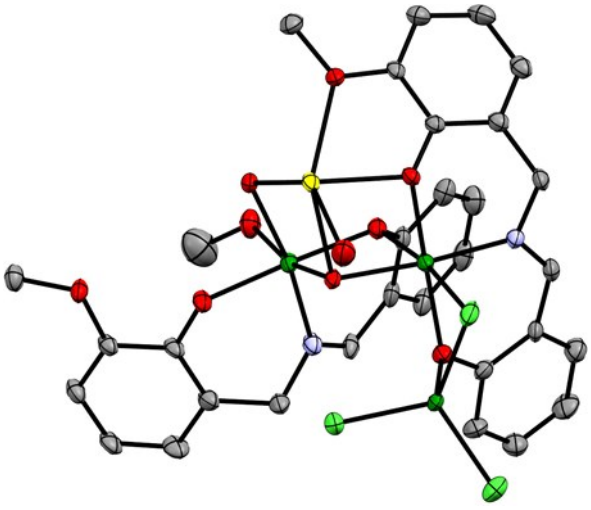

Fig. S5 The ORTEP plot of asymmetric unit in **2** with displacement ellipsoids drawn at 50% probability level (right). The hydrogen atoms were omitted for clarity.

Table S7 Selected bond distances (Å) of **2**

Atom 1	Atom 2	Distance		Atom 1	Atom 2	Distance
Ni1	O3	2.024(6)		Ni3	Cl1	2.320(3)
Ni1	O2	2.035(6)		Ni3	Cl2	2.258(3)

Ni1	O9	2.097(6)		Ni3	Cl3	2.188(3)
Ni1	N1	2.011(7)		Ni3	O6	1.971(6)
Ni1	O7	2.132(5)		Dy1	O5	2.267(5)
Ni1	O8	2.072(6)		Dy1	O2	2.263(5)
Ni2	Cl1	2.658(3)		Dy1	O4	2.532(6)
Ni2	O5	2.019(5)		Dy1	O1	2.516(5)
Ni2	O3	2.078(6)		Dy1	O10	2.356(7)
Ni2	O6	2.021(6)		Dy1	O7	2.307(5)
Ni2	N2	1.998(7)		Dy1	O7	2.368(5)
Ni2	O8	2.046(5)		Dy1	O8	2.362(5)

Table S8 Selected bond angles (°) of **2**

Atom 1	Atom 2	Atom 3	Angles		Atom 1	Atom 2	Atom 3	Angles
O3	Ni1	O2	177.2(2)		O5*	Dy1	O10	92.9(2)
O3	Ni1	O9	90.8(2)		O5*	Dy1	O7*	100.39(18)
O3	Ni1	O7	101.0(2)		O5*	Dy1	O7	159.94(18)
O3	Ni1	O8	82.1(2)		O5*	Dy1	O8*	70.94(18)
O2	Ni1	O9	91.4(3)		O2	Dy1	O5*	128.7(2)
O2	Ni1	O7	80.8(2)		O2	Dy1	O4*	74.8(2)
O2	Ni1	O8	96.1(2)		O2	Dy1	O1	65.58(18)
O9	Ni1	O7	88.2(2)		O2	Dy1	O10	102.2(2)
N1	Ni1	O3	88.0(3)		O2	Dy1	O7*	99.0(2)
N1	Ni1	O2	90.3(2)		O2	Dy1	O7	71.39(19)
N1	Ni1	O9	91.0(3)		O2	Dy1	O8*	160.26(19)
N1	Ni1	O7	171.0(2)		O1	Dy1	O4*	73.33(19)
N1	Ni1	O8	100.5(3)		O10	Dy1	O4*	144.8(2)
O8	Ni1	O9	166.2(2)		O10	Dy1	O1	73.7(2)
O8	Ni1	O7	81.6(2)		O10	Dy1	O7	80.9(2)
O5	Ni2	Cl1	90.52(17)		O10	Dy1	O8*	76.4(2)
O5	Ni2	O3	88.9(2)		O7	Dy1	O4*	128.27(18)
O5	Ni2	O6	170.7(2)		O7*	Dy1	O4*	74.41(19)

O5	Ni2	O8	82.7(2)		O7	Dy1	O1	122.90(18)
O3	Ni2	Cl1	170.47(17)		O7*	Dy1	O1	146.9(2)
O6	Ni2	Cl1	80.33(19)		O7*	Dy1	O10	139.3(2)
O6	Ni2	O3	99.9(2)		O7*	Dy1	O7	73.6(2)
O6	Ni2	O8	95.6(2)		O7*	Dy1	O8*	72.10(19)
N2	Ni2	Cl1	89.7(2)		O8*	Dy1	O4*	117.80(18)
N2	Ni2	O5	91.0(2)		O8*	Dy1	O1	130.83(18
N2	Ni2	O3	99.8(3)		O8*	Dy1	O7	89.04(18)
N2	Ni2	O6	90.3(2)		Ni3	Cl1	Ni2	76.98(9)
N2	Ni2	O8	173.6(2)		Ni2	O5	Dy1*	105.2(2)
O8	Ni2	Cl1	89.05(17)		Ni1	O3	Ni2	97.3(2)
O8	Ni2	O3	81.4(2)		Ni1	O2	Dy1	107.2(2)
Cl2	Ni3	Cl1	105.76(11)		Ni3	O6	Ni2	102.3(3)
Cl3	Ni3	Cl1	119.21(13)		Ni2	O8	Ni1	96.8(2)
Cl3	Ni3	Cl2	110.77(13)		Ni2	O8	Dy1*	101.0(2)
O6	Ni3	Cl1	90.47(19)		Ni1	O8	Dy1*	102.1(2)
O6	Ni3	Cl2	115.62(19)		Ni1	O7	Dy1	100.5(2)
O6	Ni3	Cl3	113.7(2)		Ni1	O7	Dy1*	102.1(2)
O5*	Dy1	O4*	65.63(18)		Dy1	O7	Dy1*	106.4(2)
O5*	Dy1	O1	72.52(18)					

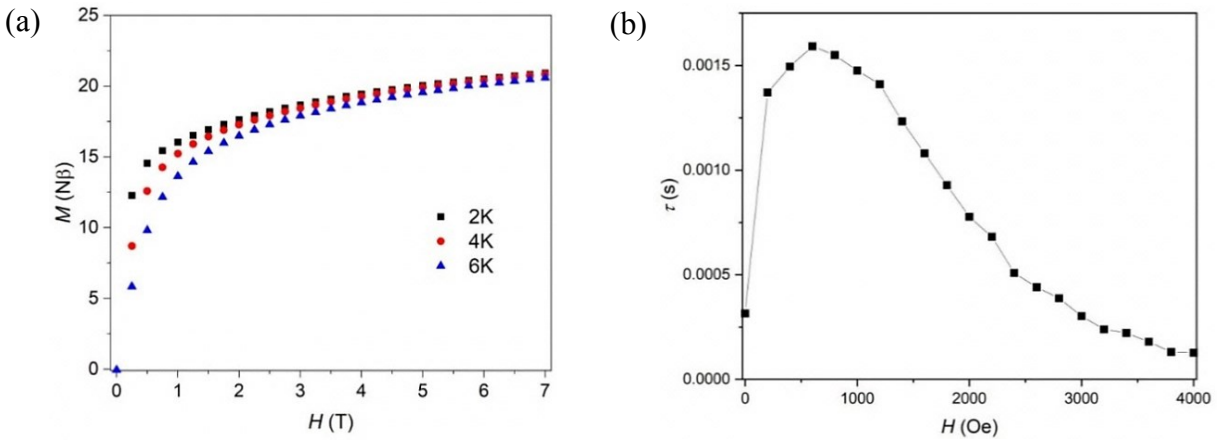

Fig. S6 (a) Magnetization *vs.* field data at 2, 4 and 6 K for complex **2**. (b) Relaxation times (τ) as a function of the applied field (H) for complex **2**, showing the optimum dc field as 600 Oe.

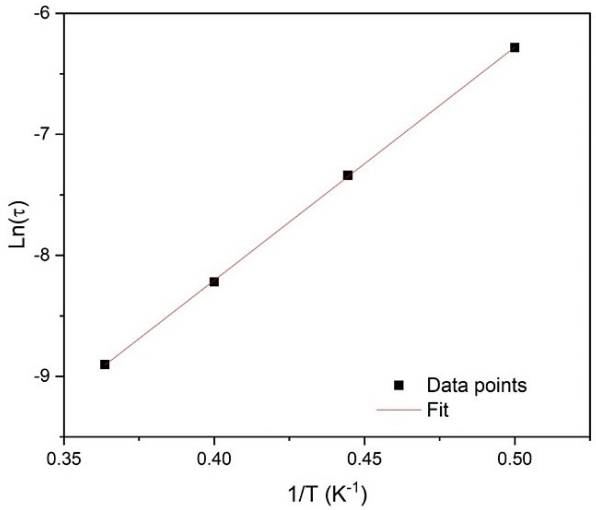

Fig. S7 Arrhenius plot ($\ln\tau$ *vs.* $1/T$) of the temperature-dependence of the relaxation rate (H_{dc} = 600 Oe) for complex **2** yielding τ_0 = 1.22 (0.07) x10^{-7} s and U_{eff} = 19.3 (0.1) K.

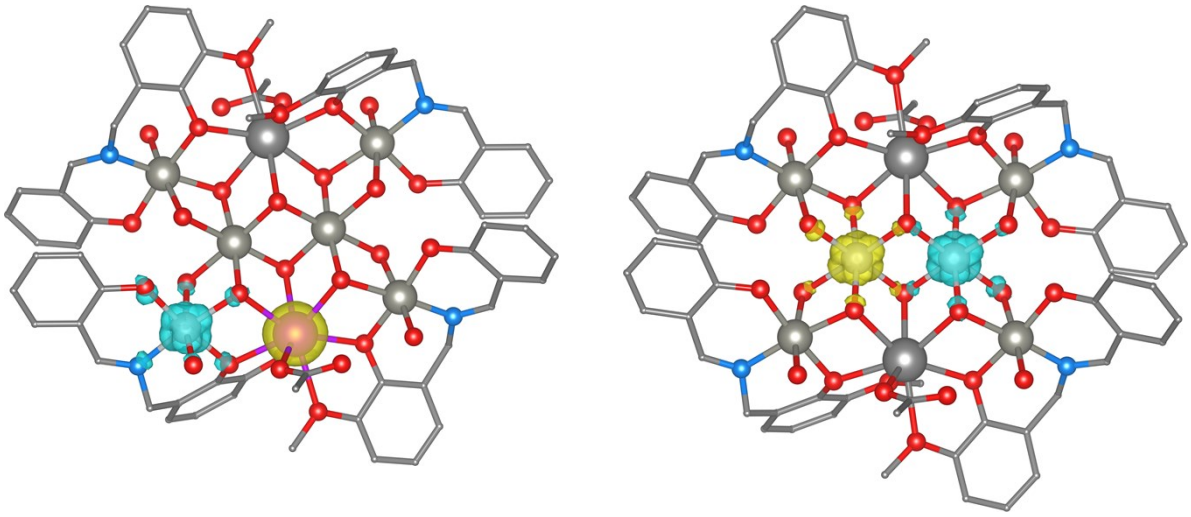

Fig. S8 The calculated spin density of the broken-symmetry spin state distribution using PBE0 functional for Gd1-Ni1 (*left*) and Ni3-Ni3* (*right*) interactions in **1**. Positive and negative spin density is represented by yellow and cyan surfaces, respectively. The isodensity surfaces are plotted with the cut-off value of $0.01ea_0^{-3}$. Hydrogen atoms are omitted for clarity.

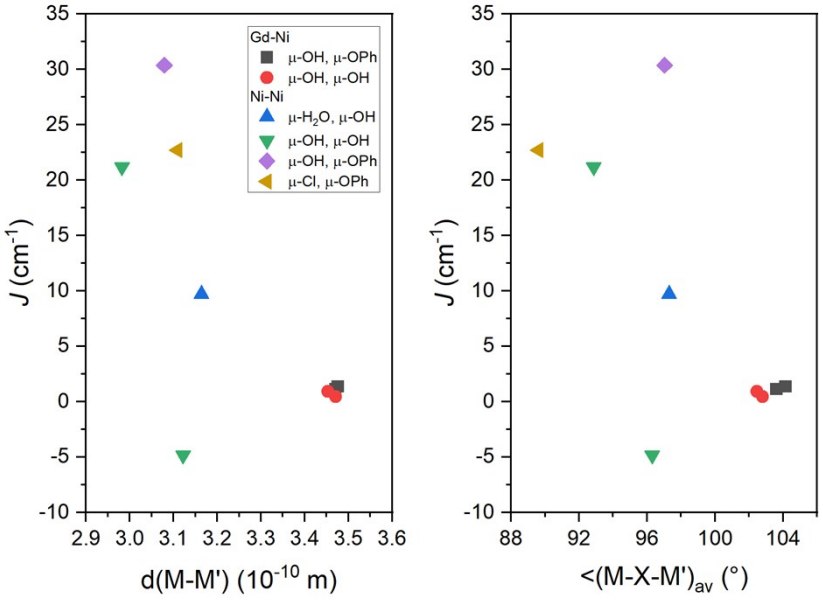

Fig. S9 The variation of *J*-parameters calculated by B3LYP functional for compounds **1** and **2** for various bridging modes.

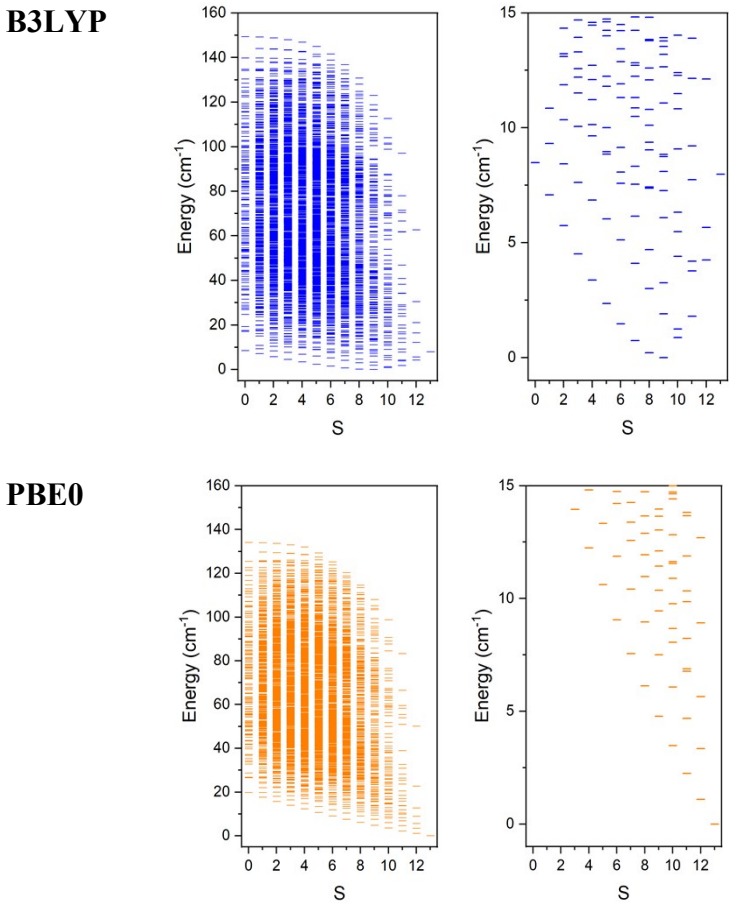

Fig. S10 The calculated spin energy levels of **1** showed as blue lines for B3LYP's derived *J*-parameters and as orange lines for PBE0's derived *J*-parameters.

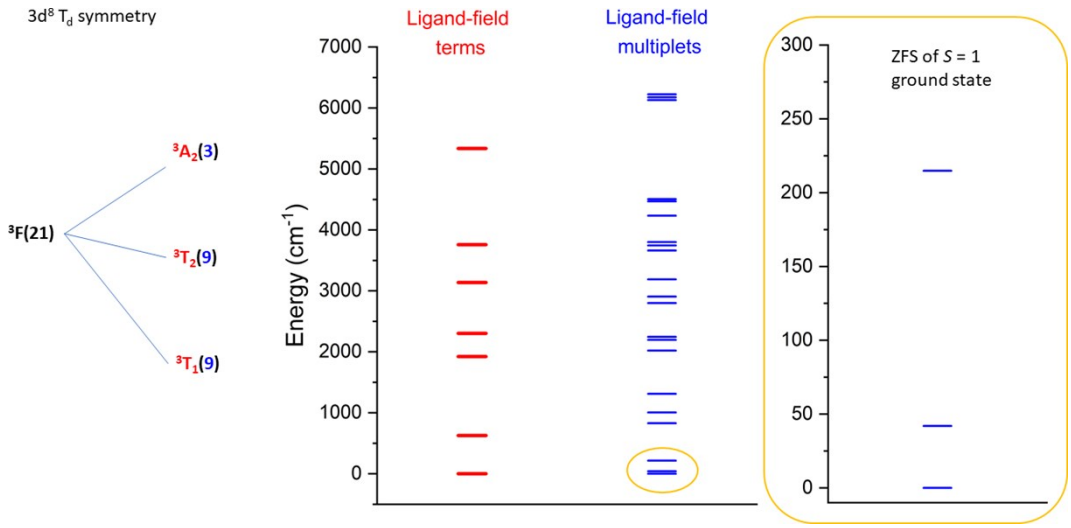

Fig. S11 *Left*: scheme of splitting of ^{3}F term of Ni^{II} ion in tetrahedral symmetry. *Middle*: CASSCF calculations for Ni3 atom of **2** showing the ligand field terms (red) and ligand field multiplets (blue) originating from ^{3}F term. *Right*: the splitting of triplet ground states with SINGLE_ANISO calculated parameters: D = -194 cm^{-1} and E = 21.0 cm^{-1}.

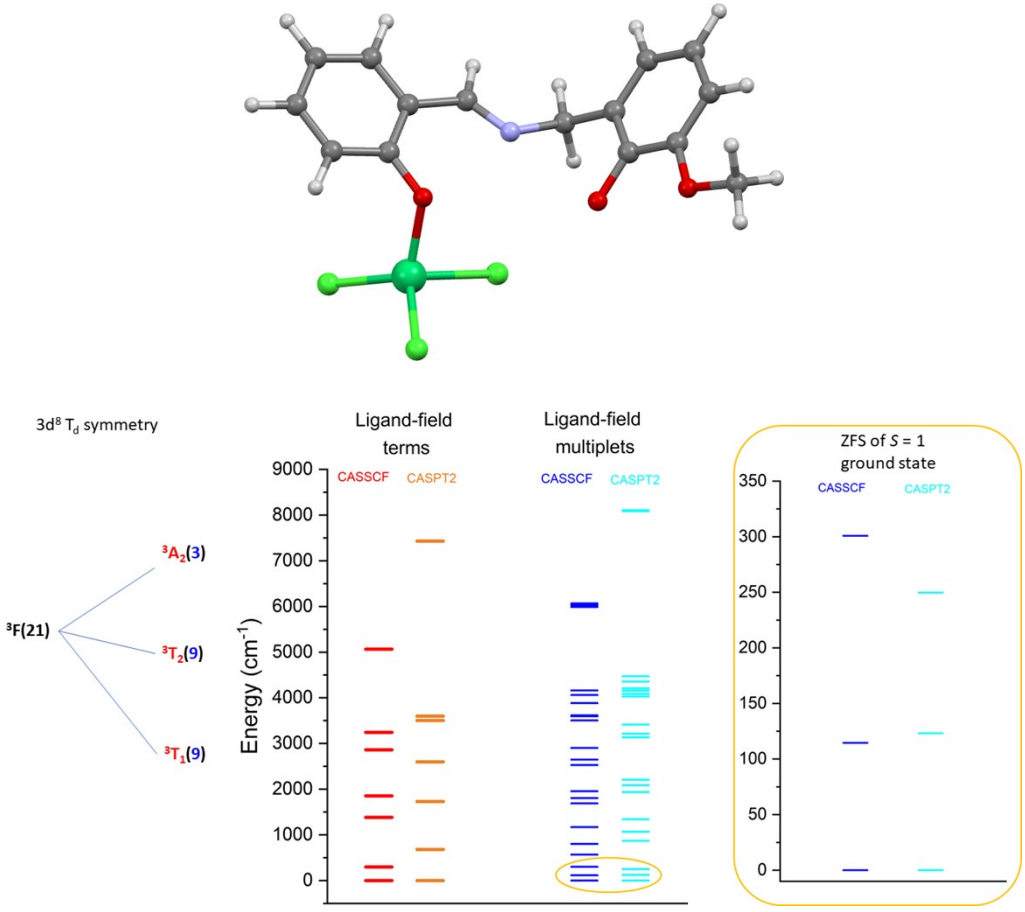

Fig. S12 *Left*: scheme of splitting of ^{3}F term of Ni^{II} ion in tetrahedral symmetry. *Middle*: CASSCF and CASSCF/CASPT2 calculations with ANO-RCC-VTZP basis set used for all atoms on small molecular fragment of **2** comprising Ni3 atom depicted at top and showing the ligand field terms (red/orange) and ligand field multiplets (blue/cyan) originating from ^{3}F term. *Right*: the splitting of triplet ground states with SINGLE_ANISO calculated parameters: D = -243 cm^{-1} and E = -57.3 cm^{-1} for CASSCF; D = -188 cm^{-1} and E = -61.6 cm^{-1} for CASSCF/CASPT2.

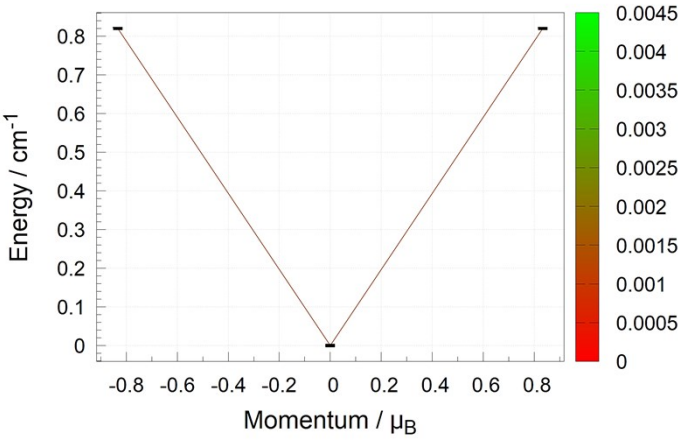

Fig. S13 Magnetization blocking barrier of [Zn_6Dy_2] of **2** calculated with POLY_ANISO taking into the account only dipolar interactions between two ground state Kramers doublets of both Dy atoms. The magnetic relaxation path, outlining the blocking barrier, is traced by the red-green lines scaling the transition magnetic dipole matrix elements between the connected multiplet states.

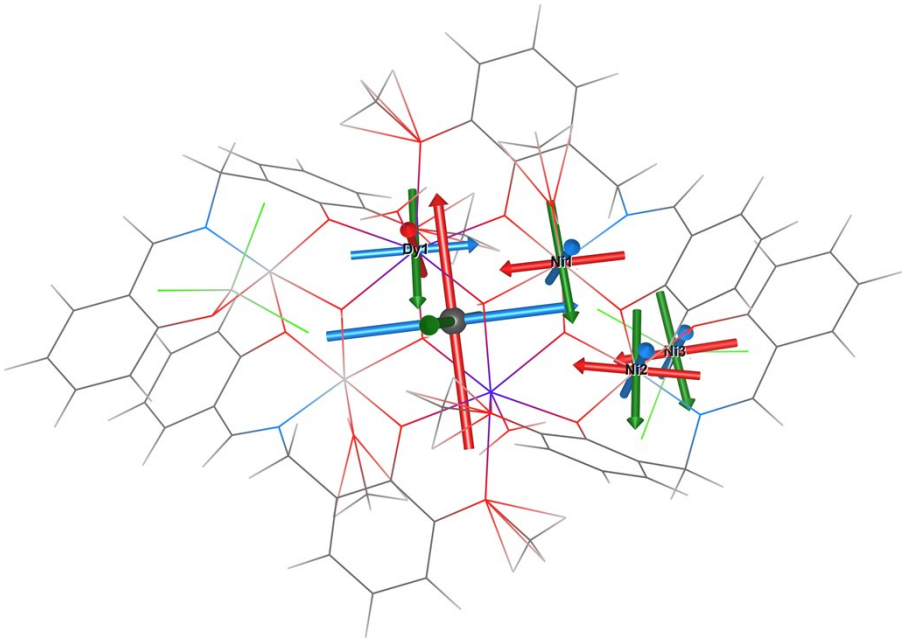

Fig. S14 The local *D* anisotropy axes of Ni atoms and local *g*-anisotropy axes of Dy atom resulting from SINGLE_ANISO calculations together with molecular anisotropy axes of ground state *g*-anisotropy axes (S_{eff} = 1/2) resulting from POLY_ANISO calculations. Color coding: x-axis – red color, y-axis – green color, z-axis – blue color. The molecular *g*-tensor axes are located in the center of molecule and are plotted with longer arrows.

References

S1. R. A. Coxall, S. G. Harris, D. K. Henderson, S. Parsons, P. A. Tasker and R. E. P. Winpenny, *J. Chem. Soc. Dalton Trans*., 2000, 2349–2356.

S2. M. Pinsky and D. Avnir, *Inorg. Chem*., 1998, **37**, 5575–5582.

S3. D. Casanova, M. Llunell, P. Alemany and S. Alvarez, *Chem. Eur. J*., 2005, **11**, 1479–1494.